18th Australasian Fluid Mechanics Conference
Launceston, Australia
3-7 December 2012

Direct numerical simulation of horizontal convection driven by differential heating

B. Gayen, R. W. Griffiths, G. O. Hughes and J. A. Saenz

Research School of Earth Sciences
The Australian National University, Canberra ACT 0200, AUSTRALIA

Abstract

A numerical study based on three-dimensional direct numerical simulations are performed to investigate horizontal thermal convection in a long channel at a large Rayleigh number, *Ra*. Differential thermal forcing is applied at the bottom boundary over two equal regions. The steady-state circulation is achieved after the net heat flux from the boundary becomes zero. A stable thermocline forms above the cooled base and is advected over the heated part of the base, confining small-scale three-dimensional convection to the heated base and end wall region. At the end-wall a narrow turbulent plume rises through the full depth of the channel. The less energetic return flow is downward in the interior, upon which eddy motions are imposed. This work, for the first time, focuses on the three dimensional instabilities and structures of the flow. The conversions of mechanical energy are examined in different regions of the flow (boundary layer, plume and interior) and help to understand overall circulation dynamics.

Introduction

Horizontal convection (HC) is driven by a horizontal difference in temperature or heat flux at a single horizontal boundary of a fluid. In a thermally equilibrated state net heat flux over the boundary is zero and circulation cell involves a horizontal boundary flow, turbulent plume motion at the end wall and weak interior return flow, covers the entire the flow domain [5]. HC is of interest given [13]'s proposed model of the meridonial overturning circulation (also known as global thermohaline circulation) based on a convective flow which is driven by a horizontal surface temperature gradient.

Experimental observations [10] show a single convecting cell of marked asymmetric structure. Based on a buoyancy-viscous balance gave scaling the boundary layer thickness and the Nusselt number. Later, [7] and [1] revisited HC at higher Ra with small aspect ratio. In their experiment, an unsteady, eddying overturning circulation exists and establishes the density stratification throughout the depth of the box. It is clear that HC is remains an interesting problem in the context of its probable role in global circulation of the ocean where the net heating and cooling is applied over the sea surface at low and high latitudes, respectively.

Nevertheless, contracting opinions exist among theoretical oceanographers [8, 16, 9, 3, 6] regarding the capability of HC, or more precisely surface buoyancy forcing, to contribute to the circulation, some appealing to wind and tides as the only sources of mechanical energy to maintain the observed stratification in the abyssal ocean and drive the circulation. [9] have derived expression for volume integrated dissipation rate and an upper bound on this at infinite Ra which is later supported by [6] using two-dimensional numerical simulation. [9] has also restricted the HC from being a turbulent flow on the basis vanishing dissipation vanishing diffusivity (hence at infinite Rayleigh number). On the other hand recent 3D numerical studies by [11] provide a different view about the dynamical nature of HC, based on the geometrical statistics that indicate a turbulent flow.

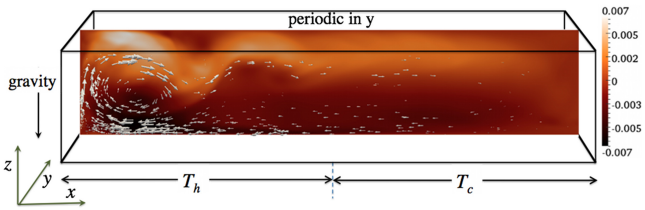

Figure 1: Schematic of the domain used for the simulation: the hot plate of temperature $T_h = 40\,^{\circ}C$ on the left-half of the base ($0 \le x < L/2$) and the cold plate temperature of $T_c = 10\,^{\circ}C$ on the right half of the base ($L/2 < x \le L$). Superposed is a snapshot from the numerical of the horizontal velocity field, u(m/s) in x-z plane at thermally equilibrated state.

Recently, [4], [14] provide the framework in which energy conversions in the global ocean can be understood. It is still unclear what drives the circulation observed previously in the numerous laboratory experiments [10, 7, 1] and the fully resolved 3D DNS simulations [11] given the strong constraint on total dissipation and on the net mount of conversion from potential to kinetic energy. We therefore, use DNS to the examine energetics of convection at large Rayleigh number.

Formulation of the problem

The simulation corresponds closely to conditions used in the laboratory experiments by [7]. The channel domain has length $L = 1.25\,m$, height $H = 0.2\,m$ and width $W = 0.05\,m$ (in which direction the domain is assumed to be periodic). Constant and uniform temperatures $T_h = 40\,^{\circ}C$ and $T_c = 10\,^{\circ}C$ are each applied over half of the base as shown in figure 1. All other boundaries are assumed to be adiabatic. The working fluid is water with kinematic viscosity $\nu = 10^{-6}\,m^2/s$ and thermal diffusivity, $\kappa_T = 2 \times 10^{-7}\,m^2/s$.

Governing equations

Direction numerical simulation (DNS) is used to solve dimensionless the continuity, Navier-Stokes and temperature equations for linear Boussinesq fluid:

$$\nabla \cdot \mathbf{u} = 0, \quad \frac{D\mathbf{u}}{Dt} = -\nabla p^* + Pr\nabla^2\mathbf{u} + RaPrT^*\mathbf{k}, \quad \frac{DT}{Dt} = \nabla^2 T \tag{1}$$

where the dimension quantities $\mathbf{u} = (u, v, w)$ is the velocity field and and T is temperature, p^* is deviation from the background hydrostatic pressure, T^* denotes the deviation from the background state and t is time. The governing equations have three nondimensional parameters: Rayleigh number Ra, Prandtl number Pr and aspect ratio, A_r , where

$$Ra \equiv \frac{\alpha_T g \Delta T_d H^3}{\nu\kappa_T} \quad , \quad Pr \equiv \frac{\nu}{\kappa_T} \quad , \quad A_r = H/L. \tag{2}$$

Here dimensional quantities in the problem are horizontal temperature difference at the bottom boundary ΔT_d, length of the channel, L, H and the fluid properties: molecular viscosity, ν,

thermal diffusivity, κ_T , thermal expansion coefficient, α_T, and reference density, ρ_0.

The variables are nondimensionalized as follows:

$$\left.\begin{aligned} t = \frac{t_d}{L^2/\kappa_T}, \mathbf{x} = (x,y,z) = \frac{(x_d,y_d,z_d)}{L}, p^* = \frac{p_d^*}{\rho_o \kappa_T^2/L^2}, \\ \mathbf{u} = (u,v,w) = \frac{(u_d,v_d,w_d)}{\kappa_T/L}, \ T = \frac{T_d}{\Delta T_d}. \end{aligned}\right\} \quad (3)$$

Numerical method

The simulations use a mixed spectral/finite difference algorithm. Periodicity is imposed in the spanwise, $y-$ direction and derivatives are evaluated with a pseudo-spectral method. The grid is staggered in the vertical and streamwise directions and the corresponding derivatives are computed with second-order finite differences. A low-storage third-order Runge-Kutta-Wray method is used for time stepping, except for the viscous terms which are treated implicitly with the alternating direction implicit (ADI) method. The code has been parallelized using the message passing interface (MPI). Variable time stepping with a fixed Courant-Friedrichs-Lewy (CFL) number of 1.0 is used. Time steps are the order of $10^{-1}\,s$.

Initialization & Domain resolution

The simulation is initialized with an isothermal tank of water at temperature, $T_{in} = 35^\circ C$ and no motion the tank interior. Small amount of white noise is applied at initial time after damping outside the bottom boundary. The Prandtl number is chosen to be $Pr = 5$. Based values values of the dimensional parameters Rayleigh number of the flow is $Ra = 5.86 \times 10^{11}$. The computational grid has $513 \times 128 \times 257$ points in the x, y and z directions, respectively. We have checked the grid resolution by comparing with the Batchelor scale $\eta_b \sim Pr^{-1/2}(\nu^3/\varepsilon)^{1/4}$. We have followed the criteria $l/\eta_b \leq \pi$ as proposed by [12]. Here, l is the resolution any given direction. Resolution in the spanwise direction is also confirmed by examining scalar dissipation spectra, $2\kappa k^2 E_{\Theta'}$ (shown in figure 2) as a function of $\eta_b k$ at three different locations in the domain: inside the bottom boundary layer, the bottom and upper part of the end wall plume. The present simulations are well resolved $k_{y,max}\eta_b \sim 2$.

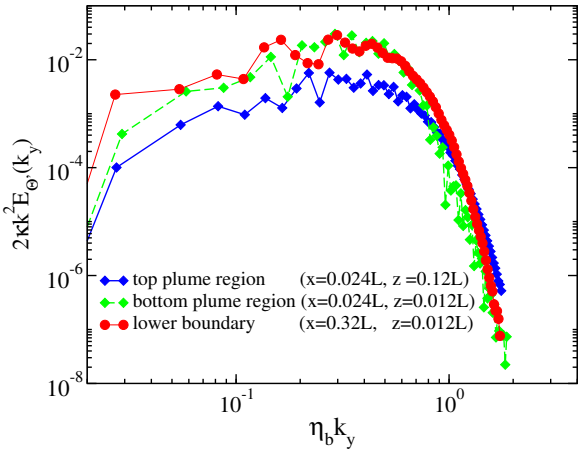

Figure 2: k_y spectra of the temperature fluctuations, Θ' at three different locations inside the domain. Data are taken at thermally equilibrated state.

The approach to the stationary state solution convergence was monitored using a time series of the average temperature in the tank and also the total heat flux leaving through the bottom base. The solution was judged to have reached thermal equilibrium when the net heat flux into the tank was less than 1% of sum of magnitudes of the individual the heat flux acting from the bottom surface, i.e.

$$\left|\int_0^L\int_0^W \frac{\partial T}{\partial z}dydx\right| \Big/ \int_0^L\int_0^W \left|\frac{\partial T}{\partial z}\right| dydx \leq 0.01 \qquad \text{at } z\text{=}0 \quad (4)$$

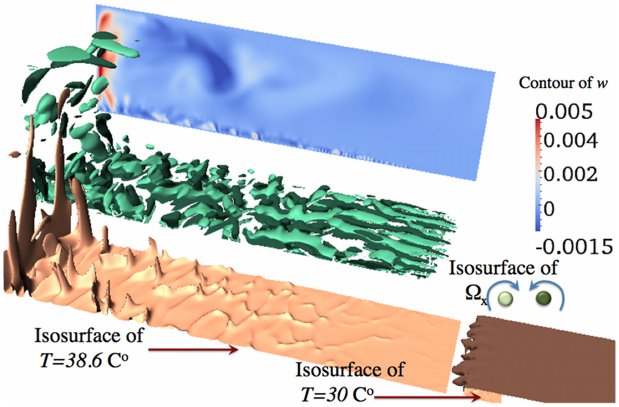

Figure 3: Three dimensional visualization of the thermally-equilibrated flow. The vertical slice shows the contours of the vertical velocity at $y = 0.05\,m$. Iso-surfaces ($\pm 0.3\,s^{-1}$) of streamwise vorticity, Ω_x as shown at the middle panel and iso-surfaces of temperature are shown in the front panel. The mean interior temperature at equilibrium is $\sim 38.5^\circ C$.

Results

Flow structures

Thermally equilibrated state was reached after a time, $t = 8\,hr$ in the simulation and flow field is similar to that observed in previous experimental studies [10, 7]. A large scale overturning circulation fills the channel and consists of a stably-strafied boundary layer above the base which is feeding into a strong, unsteady and narrow plume against the endwall at the heated end. Fluid leaving the plume in an outflow against the upper boundary enters the interior, which is characterized by broad and gradual downwelling.

Details examination of the flow structures inside the boundary layer is illustrated in figure 3 at steady state ($t \sim 10\,hr$). The stable thermocline is maintained above the cooled base and is advected across the heated half of the base, capping the small scale convection. But the convection driven by bottom heating erodes the stable temperature gradient from the beneath. Coherent rolls which are shown by isosurface of counter-rotating streamwise vortices, $\Omega_x = [\nabla \times \mathbf{u}] \cdot \mathbf{i}$, are aligned with the boundary layer flow near the middle of the bottom surface. These coherent rolls survive for a small distance of $\sim 70 - 100$ mm from the cold base. Similar streamwise convection rolls were observed in the previous laboratory experiments [7] with an imposed heat influx and a constant bottom base temperature. These vortices have a strong impact on the temperature field by developing spanwise corrugations of isotherms as shown by temperature isosurface of magnitude, $T = 30^\circ C$ in figure 3. (Recently, [2] have observed a similar type of three dimentional convective roll associated with spanwise density corrugation during the convective instability of internal waves at a critical slope.) These counter rotating vortices interact and merge with each other approximately 350-400 mm away from the end wall over the heated base, resulting in fully three dimensional complex structures.

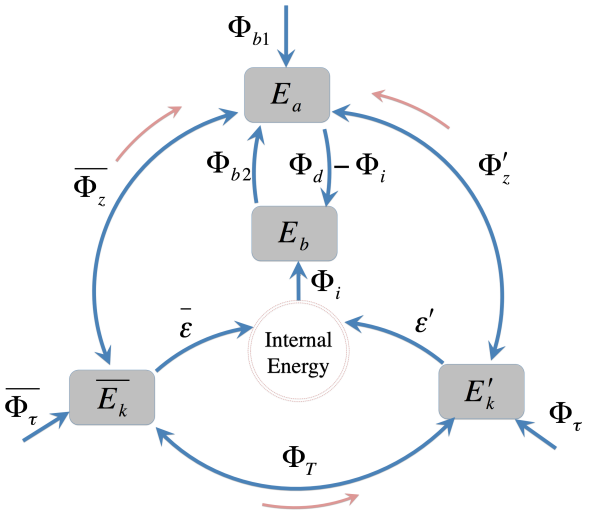

Figure 4: Schematic diagram showing the various forms and transformations of mechanical energy in a density-stratified flow of a linear Boussinesq fluid [4]. Quantities associated with mean flow are denoted by over bar and those associated with fluctuating components. are primed. The energy within a fixed volume is stored as kinetic energy, E_k, available potential energy, E_a, background potential energy, E_b and internal energy. External energy is supplied to the flow by surface stresses at a rate $\overline{\Phi}_\tau$ and by net buoyancy input at any level at a rate Φ_{b1}. Energy exchanges between E_a and E_k occurs via buoyancy fluxes, $\overline{\Phi}_z$ and Φ'_z. Conversion between the mean and turbulent kinetic energy is caused by mean shear Φ_T. $\bar{\varepsilon}$ and ε' are the rates of viscous dissipation from the kinetic energy reservoir. Transfers between reservoirs of the available and the background potential energy include irreversible mixing, Φ_d, release of internal energy by molecular diffusion, Φ_i and differential buoyancy input at any level, Φ_{b2}. In case where the rates of transformation can be bidirectional, an additional arrow denotes a positive quantity.

Small convective plumes become obvious features and are restricted by the overlying stable gradient of the boundary layer as shown by isosurface of temperature, $T = 38.6\,^\circ C$ in the figure 3. These three dimensional convective mushroom structures, which penetrate to greater heights nearer the end wall, are inclined slightly leftward due to the influence of bottom boundary flow. Eventually, at the end wall, the stable gradient has been eroded and the convective elements join a turbulent plume through the full depth of the channel. Vertical temperature gradient is weak but positive in the interior with a variation of $\sim 0.02\,^\circ C$ over the upper three-quarters of the depth. The buoyancy frequency N decreases by two order of magnitudes from the boundary layer to interior (as previously shown by 2D solution and experiments by [7])

Flow energetics

Following [15] and [4], we define for a linear Boussinesq fluid the mean kinetic energy, $\overline{E}_k = \rho_0/2 \int \overline{u}_i \overline{u}_i dV$, the turbulent kinetic energy, $E'_k = \rho_0/2 \int u'_i u'_i dV$, the potential energy, $E_p = g \int z \rho dV$, the background potential energy, $E_b = g \int z^* \rho dV$ and the available potential energy, $E_a = E_p - E_b$, where $z^* = z^*(\rho)$ is the height at which a parcel of density ρ would reside if the entire density field is allowed to relax adiabatically to equilibrium (the background state). $\overline{(\cdot)}$, denotes an average of the quantity calculated by averaging over the spanwise direction. The rates at which mechanical energy is transfered between these form is shown schematically in figure 4 (see [4] for more details.)

For thermally-quilibrated horizontal convection, the only non-zero forcing term in figure 4 is $\Phi_{b2} = g\kappa_T \oint z^*(\partial\rho/\partial x_j) n_j dS$ (i.e. $\overline{\Phi}_\tau = \Phi'_\tau = \Phi_{b1} = 0$). We proceed to evaluate the remaining terms from the the simulation: $\Phi_T = -\rho_0 \int (\partial \bar{u}_i/\partial x_j) \overline{u'_i u'_j} dV$, $\overline{\Phi}_z = g \int \bar{\rho} \bar{w} dV$, $\Phi'_z = g \int \overline{\rho' w'} dV$, $\bar{\varepsilon} = \rho_0 \nu \int (\partial \bar{u}_i/\partial x_j)^2 dV$, $\varepsilon' = \rho_0 \nu \int (\partial u'_i/\partial x_j)^2 dV$, $\Phi_d = -g\kappa_T \int (dz^*/d\rho)(\partial\rho/\partial x_j)^2 dV$ and $\Phi_i = -g\kappa_T A(\overline{\rho}_{top} - \overline{\rho}_{bottom})$, which take the mean values given in table 1.

Φ_T	$\bar{\Phi}_z$	Φ'_z	$\bar{\varepsilon}$	ε'	Φ_i	Φ_d	Φ_{b2}
0.12	-2.10	-1.42	1.98	1.54	3.52	45.5	−45.5

Table 1: Table for various energy conversion terms ($\times 10^{-7}$) integrated over the whole volume of the box. Values are in Watt.

The mean dissipation, $\bar{\varepsilon}$, and the mean buoyancy flux, $\overline{\Phi}_z$, are the dominant terms in the KE budget. Mean buoyancy flux oscillates more, compared to $\bar{\varepsilon}$, around its mean values over the steady-state. For the present case the surface buoyancy flux Φ_{b2} is the dominant source of available potential energy, and is balanced by the rate dissipation due to irreversible mixing i.e. $\Phi_{b2} = \Phi_d$. This exact balance also has been predicted by [14] and [4] .

The total dissipation $(\bar{\varepsilon} + \varepsilon')$ is equal to Φ_i, which is equal to total $APE - KE$ conversion (total buoyancy flux, $\overline{\Phi}_z + \Phi'_z$). As Φ_i is dependent on the difference of the averaged value of buoyancy $\Delta\overline{\rho}$ between the top and the bottom surface multiplied by thermal diffusivity, κ_T, it must equal the total dissipation, which must equal the total conversion from $APE - KE$. We argue that [9]'s conjecture of non turbulence nature of horizontal convection at the limit of $\kappa_T \to 0$ is misleading. At infinite Rayleigh number, $Ra \to \infty$ based on $\kappa_T \to 0$, $\nu \to 0$, the imposed surface buoyancy flux also vanishes ($\Phi_{b2} \to 0$) and we end up with with zero dissipation from the kinetic energy reservoir and zero energy influx for the buoyancy field, ($\Phi_{b2} = 0$). (Based on the same argument the limit of $\nu \to 0$, dissipation from the wind field also becomes zero, Ref. Eqn. (1.6) by [3]). In contrast, at a finite value of surface buoyancy flux, available potential energy is created and returned to the background potential energy via irreversible mixing. The rate generation of APE and irreversible mixing (Φ_d) are one order of magnitude larger than box integrated dissipation (and Φ_i). This demonstrates that consideration of the KE budget alone overlooks the dominant physics of the flow.

We have also examined APE to KE conversion in four of the flow regions: (1) lower boundary layer, (2) plume region, (3) upper boundary region and (4) interior. In particular, comparable and oppositely-signed rates of APE to KE conversion take place in the plume and interior regions and each is more than three orders of magnitude greater than the other terms in the kinetic energy budget. This reveals that integrating over the whole volume obscures physically important APE to KE conversion.

The turbulent mixing efficiency for HC is defined as $\eta = (\Phi_d - \Phi_i)/(\Phi_d - \Phi_i + \varepsilon) = 1 - \Phi_i/\Phi_d$ and for the present simulation of $\eta \sim 0.927$. Note that previous definition of the overall mixing efficiency as $\eta = \Phi_d/(\Phi_d + \Phi_i)$ by [11] is misleading, because it will reflect the highest efficiency of $\eta \to 1$ even for a stationary stratified fluid, where $\Phi_i \to 0$.

Conclusion

Results based on 3D direct numerical simulation are presented here at large Raleigh number ($Ra \sim O(10^{12})$) for horizontal

convection in a long channel driven by differential heating over the bottom surface. A strong circulation exists over the entire water column, similar to the earlier experimental observations. Convective mixed layer is formed over the heated base by flow parallel role instability and breakdown to small-scale 3D plumes. At the end wall a large turbulent plume, fed by the bottom convective mixed layer, penetrates through the full depth of channel. Importantly, the simulation shows how horizontal convection can be vigorous while satisfying the constraint of [9]. The results shows large conversions of available potential energy to kinetic energy by buoyancy flux in the end wall plume and the reverse in the interior of the circulation. A large value of turbulent mixing efficiency, $\eta \sim 0.927$ claims that horizontal convection is highly efficient in the sense that a strong overturning circulation and irreversible mixing occurs with minimal viscous dissipation.

Acknowledgement

Numerical computations were conducted using the Australian National Computa- tional Infrastructure, ANU. This work was supported by Australian Research Council grants DP1094542 and DP120102744. G. O. H. was supported by ARC Future Fellowship FT100100869.

*

References

[1] M. A. Coman, R. W. Griffiths, and G. O. Hughes. Sandstrom's experiments revisited. *J. Mar. Res.*, 64:783–796(14), 2010.

[2] B. Gayen and S. Sarkar. Turbulence during the generation of internal tide on a critical slope. *Phys. Rev. Lett.*, 104:218502, 2010.

[3] J. Hazewinkel, F. Paparella, and W. R. Young. Stressed horizontal convection. *J. Fluid Mech.*, 692:317–331, 2012.

[4] G. O. Hughes, A. McC Hogg, and R. W. Griffiths. Available potential energy and irreversible mixing in the meridional overturning circulation. *J. Phys. Oceanogr.*, 39(12):3130–3146, 2009.

[5] Graham O. Hughes and Ross W. Griffiths. Horizontal convection. *Annu. Rev. Fluid Mech.*, 40(1):185–208, 2008.

[6] M. Ilicak and G. K. Vallis. Simulations and scaling of horizontal convection. *Tellus*, 64:9 – 16, 2012.

[7] C. Mullarney, R. W. Griffiths, and G. O. Hughes. Convection driven by differential heating at a horizontal boundary. *Journal of Fluid Mechanics*, 516:181–209, 2004.

[8] Walter Munk and Carl Wunsch. Abyssal recipes ii: energetics of tidal and wind mixing. *Deep-Sea Res. I*, 45(12):1977 – 2010, 1998.

[9] F. Paparella and W. R. Young. Horizontal convection is non-turbulent. *J. Fluid Mech.*, 466:205–214, 2002.

[10] H.T. Rossby. On thermal convection driven by non-uniform heating from below: an experimental study. *Deep Sea Res.*, 12(1):9 – 16, 1965.

[11] A. Scotti and B. White. Is horizontal convection really "non-turbulent"? *Geophys. Res. Lett.*, 38(21), 2011.

[12] R. J. A. M. Stevens, R. Verzicco, and D. Lohse. Radial boundary layer structure and nusselt number in rayleigh-bénard convection. *J. Fluid Mech.*, 643:495–507, 2010.

[13] Henry Stommel. On the smallness of sinking regions in the ocean. *Proc. Natl. Acad. Sci.*, 48(5):766–772, 1962.

[14] R. Tailleux. On the energetics of stratified turbulent mixing, irreversible thermodynamics, boussinesq models and the ocean heat engine controversy. *J. Fluid Mech.*, 638:339–382, 2009.

[15] K. B. Winters, P. N. Lombard, J. J. Riley, and E. A. D'Asaro. Available potential energy and mixing in density-stratified fluids. *J. Fluid Mech.*, 289:115–128, 1995.

[16] Carl Wunsch and Raffaele Ferrari. Vertical mixing, energy, and the general circulation of the oceans. *Annu. Rev. Fluid Mech.*, 36(1):281–314, 2004.